Ocean Wave Extraction from RADARSAT Synthetic Aperture Radar Inter-Look Image Cross-Spectra

Michael Dowd

Ocean Sciences Division, Department of Fisheries and Oceans,

Biological Station, St. Andrews, N.B, Canada

Paris W. Vachon

Canada Centre for Remote Sensing,

Natural Resources Canada, Ottawa, Canada

Fred W. Dobson

Ocean Sciences Division, Department of Fisheries and Oceans,

Bedford Institute of Oceanography, Dartmouth, N.S., Canada

Richard B. Olsen

Norwegian Defence Research Establishment, Kjeller, Norway

Abstract

This study is concerned with the extraction of directional ocean wave spectra from synthetic aperture radar (SAR) image spectra. The statistical estimation problem underlying the wave-SAR inverse problem is examined in detail in order to properly quantify the wave information content of SAR. As a concrete focus, a data set is considered comprising 6 RADARSAT SAR images co-located with a directional wave buoy off the east coast of Canada. These SAR data are transformed into inter-look image cross-spectra based on two looks at the same ocean scene separated by 0.4 seconds. The general problem of wave extraction from SAR is cast in terms of a statistical estimation problem which includes the observed SAR spectra, the wave-SAR transform and prior spectral wave information. The central role of the weighting functions (inverse of the error covariances) is demonstrated, as well as the consequence of approximate (based on the quasi-linear wave-SAR transform) versus exact linearizations on the convergence properties of the algorithm. Error estimates are derived and discussed. This statistical framework is applied to the extraction of spectral wave information from observed RADARSAT SAR image cross-spectra. A modified wave-SAR transform is used to account for case-specific geophysical and imaging effects. Analysis of the residual error of simulated and observed SAR spectra motivates a canonical form for the SAR observation error covariance. Wave estimates are then extracted from the SAR spectra, including wavenumber dependent error estimates and explicit identification of spectral null spaces where the SAR contains no wave information. Band-limited SAR wave information is also combined with prior (buoy) spectral wave estimates through parameterization of the wave spectral shape and use of regularization.

1 Introduction

The potential for extracting ocean surface gravity wave information from synthetic aperture radar (SAR) images of the ocean surface is widely recognized. Satellite SAR missions, both current (e.g. ERS-2 and RADARSAT) and planned (e.g. ENVISAT, RADARSAT-2), have imaging modes dedicated to providing information on directional ocean wave spectra. Satellite-borne SAR has the potential to add significantly to the existing *in situ* global wave observing system, presently comprised of a sparse and irregularly distributed array of wave buoys. SAR derived wave spectra are expected to be useful for validation of, and assimilation into, operational wave models [6]. While it is evident that SAR holds much promise for observing the ocean wave spectrum, its full potential has yet to be realized.

The basic physical mechanisms governing SAR imaging of ocean waves are reasonably well understood [11]. A significant step forward was realized with the derivation of a closed form, nonlinear transform relating the ocean wave spectrum to the SAR image spectrum ([10], see also [14]). This wave-SAR transform has since been extended to cover the more general case of the SAR image cross-spectrum [8], [13]. However, a number of issues arise when using satellite SAR in a wave observing system. One fundamental difficulty is its inability to record wave induced modulations of the radar cross-section at high along-track (azimuth) wavenumbers; satellite-based SAR typically truncates signals associated with waves having less than 100m wavelengths in azimuth (e.g. [1]). Non-wave geophysical signals such as wind further modify this azimuth cutoff [26], [7]. This latter feature, together with speckle noise (e.g. [9]), limits the ability of the basic wave-SAR transform to account for the full variability found in observed SAR spectra. This has lead to wave-SAR transforms with case-specific modifications which absorb geophysical effects into the underlying physical parameterizations of the ensemble scattering properties of the ocean surface [15], [20].

Wave estimates from observed SAR spectra rely on inversion of the wave-SAR transform. These SAR derived wave estimates have received much attention in the context of operational wave modelling and data assimilation [6], [12]. A key feature of SAR is its concentration of wave information in specific wavenumber bands which are dependent on orbit characteristics, viewing geometry and prevailing sea surface conditions. Data assimilation methods require the ability to systematically compare wave spectral estimates from a model with those derived from SAR on a wavenumber dependent basis. At a fundamental level we must then consider the statistical problem of combining the information contained in *(i)* the observed SAR spectrum, *(ii)* the wave-SAR transform, and *(iii)* any prior estimates of the wave field such as those produced by a model. The goal is a posterior estimate of the directional ocean wave spectrum which maximizes the information content, and has quantitative estimates of uncertainty.

The purpose of this work is to extract spectral wave information from SAR. Towards this end, we develop a statistical estimation framework for wave-SAR inversion which allows for the wave information content of SAR to be quantified on a wavenumber dependent basis. As a particular focus, we examine a set of RADARSAT SAR inter-look image cross-spectra co-located with a wave buoy off the east coast of Canada. These cross-spectra are based on two images of the same ocean scene separated by a fraction of a second and offer advantages over SAR auto-spectra in terms of speckle noise reduction and the ability to resolve wave propagation direction [8]. We compute and analyse the SAR spectra in terms of their statistical properties and wave information content. A general statistical framework is developed for quantitatively examining the wave-SAR inverse problem. This approach encompasses other wave-SAR inversion studies (e.g. [8], [10], [15], [12]). Importantly, it provides for a means to compare and assess the consequences of the various (and often conflicting) assumptions made in these studies, consequences which are frequently obscured by the analytic complexity of the wave-SAR transform. Practical aspects of carrying out the statistically based inverse problem are undertaken based on the observed SAR image cross-spectra, the buoy wave spectra, and a wave-SAR transform modified to account for case-specific geophysical effects.

This paper is organized as follows. Section 2 presents SAR image cross-spectra from RADARSAT, along with co-located wave buoy spectra. In Section 3, the wave-SAR transform is briefly reviewed, and its inversion is examined in detail. Section 4 provides an application of the inversion procedure. Section 5 contains a summary and conclusions. Appendix A provides details of the wave-SAR transform and Appendix B introduces the (random-β) regression methodology central to our development of wave-SAR inversion.

2 Observations

In this section, we examine some RADARSAT SAR image spectra and co-located *in situ* buoy data collected during the 1996 March/April Ship Detection Experiment (MASDE) [24]. Wind and wave data were collected from two buoys (a MINIMET meteorological buoy and Datawell directional wave rider buoy) moored near 44.5°N, 63°W. Directional wave spectra were processed using a maximum likelihood method [18]. There were a total of 9 available SAR and buoy co-locations, but 3 of the SAR images contained little discernable wave information. This appeared to be due to low total wave energy combined with a strong azimuth component to the wave propagation direction. We ignore these cases hereafter. Details of the remaining 6 cases are summarized in Table 1.

The RADARSAT SAR data were processed into inter-look image cross spectra according to the

4

following procedure:

1. Separation into 5 individual looks separated by 293Hz.

2. For each of the pairs (1,3), (2,4), and (3,5):

    (a) extract 1024×1024 image region and detrend

    (b) calculate modifed periodgrams for 512×512 subregions using a Kaiser window

    (c) average the modified periodograms

3. Calculate raw cross-spectra by averaging the results for each of the look pairs and smooth through convolution with a Gaussian smoothing kernel.

The end result of this procedure is a set of SAR image cross-spectra which are based on a time separation of $\tau \sim 0.4$s (see [28]).

Comparison of the co-located wave and SAR spectra allows us to examine the wave modulation of the spectral properties of the normalized radar cross-section of the ocean surface. The directional ocean wave spectrum for the 6 cases are shown in Figure 1. These spectra are smooth as a result of the spectral processing of the buoy heave, pitch and roll data. The low wavenumber swell is recorded in all cases and case 1 shows a locally generated wind sea propagating in a near range direction. In our treatment of the SAR data, we emphasize its fundamental nature and make no attempt, at this stage, to correct for multiplicative speckle noise, or for the falloff of spectral density with increasing wavenumber [9], [17]. To supress large-scale, non-wave geophysical signals, such as marine boundary layer wind patterns [25], we have chosen not consider wavenumber regions corresponding to wavelengths > 300m (note that ocean surface gravity wave energy may be present at greater wavelengths, however our RADARSAT SAR spectra showed non-wave signals at these higher wavelengths). Finally, note that buoy and image spectra differ in that the former is derived from a time-averaged point measurement while the latter represents an instantaneous spatial snapshot.

The real part of the SAR cross-spectra (the coincident spectra) are shown in Figure 2. There is evidence of SAR imaging of the dominant 100-150m swell, although azimuth wavenumbers $|k_a| > 0.05$m^{-1} (i.e. <125m wavelengths) are truncated. Note that case 5 images a near-azimuth travelling wave, and in case 1 the locally generated wind sea is apparent. Peak energy of the SAR and buoy spectra are not always co-located (even after taking account of the gain characteristics of the SAR). While a dramatic reduction in speckle noise over the auto-spectra (not shown) is evident, some broad band noise still persists. In theory, speckle noise should be eliminated if it is statistically independent between looks [8].

To further examine the effect of the multi-look processing on the spectral energy and broad band noise, we re-processed case 5 into 5 looks, each separated by $\tau \sim 0.15$s. (Case 5 records a near azimuth travelling wave allowing for assessment of the low wavenumber non-wave signals in the range integrated spectrum). Figure 3 shows the range-integrated coincident spectra for different time separations. Reduction of the total energy is evident when comparing the auto-spectra ($\tau = 0$) with the cross-spectra ($\tau > 0$). With increasing time separation the total energy declines to a stable level after $\tau \sim 0.3$s seconds. This stabilization indicates that looks no longer overlap (in the frequency domain) and suggests a minimal value for τ to ensure statistical independence between looks. The remaining noise processes may be residual speckle, or may have a geophysical origin.

Information on the wave propagation direction resides in the anti-symmetry of the imaginary part of the SAR image cross-spectra (the quadrature spectra), shown in Figure 4. The overall magnitude of the quadrature spectra are generally less than the coincident spectra and are more variable. For cases 2, 4, and 6 the anti-symmetry is readily evident in the spectral regions containing wave information, but for the remaining cases it is not so clear. Coherency spectra were also calculated after correcting the auto-spectra for speckle and spectral falloff with increasing wavenumber [17]. These coherency spectra are used to separate the (coherent) wave signal from (incoherent) noise processes. Figure 5 shows the phase spectra for regions with coherency greater than 0.6 (this threshold coherency represents a type I error probability of 0.01 in a test for zero coherency [22]). In cases 1, 2, 4 and 6 the negative phase regions match the wave propagation direction. The direction of wave propagation in cases 3 and 5 are less clear. For the various cases, values for the mean phase in these wavenumber regions are quite different (for a 100m deep water wave we expect a phase of ~ 0.3 radians over the 0.4s time separation between looks). This may be explained by sampling variability coupled with the weak phase signature implied by the short time separation of the 2-look SAR imagery (see Section 3.1).

3 Theory

3.1 The Forward Map

The theoretical basis for examining the relation between the ocean wave spectrum and the SAR image spectrum is given by the closed form, integral transform first proposed by [10]. This has since been extended to the more general case of the SAR image cross-spectrum [8]. The wave-SAR transform may be represented as

$$S_{nl}(\vec{k}) = h \left\{ W(\vec{k}); c_j \right\}. \tag{1}$$

Here, $W(\vec{k})$ is the directional ocean wave spectrum. The vector wavenumber $\vec{k} = (k_r, k_a)$ is in satellite coordinates with k_r and k_a denoting the cross-track (range) and along-track (azimuth) wavenumbers, respectively. The c_j represent parameters of the wave-SAR map, some of which may be readily specified based on satellite properties and others which depend on prevailing environmental conditions (e.g. wind) which modify the scattering properties of the air-sea interface. The nonlinear operator $h\{\cdot\}$ represents the wave-SAR transform and its functional representation is given in Appendix A. $S_{nl}(\vec{k})$ is the SAR image cross-spectrum predicted using this nonlinear map.

To facililate implementation the wave-SAR transform (1) is often cast in terms of a series expansion (e.g. [10]),

$$S_{nl}(\vec{k}) = \exp\left\{-\pi \left(k_a/K_c\right)^2\right\} \sum_{i=1}^{\infty} \tilde{S}_i(\vec{k}) \tag{2}$$

where K_c is an (equivalent rectangular width) azimuth cutoff wavenumber and depends on $W(\vec{k})$ through the velocity bunching covariance function $\rho_{AA}(\vec{x})$ such that $K_c = \sqrt{\pi/\rho_{AA}(0)}$ (see Appendix A) . The $\tilde{S}_i(\vec{k})$ denote terms in the expansion with subscripts referring to the order of nonlinearity. The importance of higher order terms in (2) scales with the standard deviation of the azimuth shift due to velocity bunching and are expected to play a role for satellite platforms in which R/V exceeds 100s [14]. [15] demonstrates that the effect of nonlinearity on the SAR spectrum is manifest as spectral spreading of energy and the generation of higher order harmonics.

A useful simplification of the wave-SAR transform is the quasi-linear approximation. This is obtained by considering only the leading order term $\tilde{S}_1(\vec{k})$ in (2), i.e. that part of the transform that is a linear in $W(\vec{k})$. For the cross-spectral case this takes the form

$$S_{ql}(\vec{k}) = \exp\left\{-\pi \left(k_a/K_c\right)^2\right\} \left(\Psi(\vec{k})W(\vec{k})e^{i\omega\tau} + \Psi(-\vec{k})W(-\vec{k})e^{-i\omega\tau}\right) \tag{3}$$

where $\Psi(\vec{k})$ is defined in Appendix A and depends on the tilt, hydrodynamic and velocity bunching modulation of the radar cross section by the ocean gravity wave field. The term $e^{i\omega\tau}$ represents phase shifting of the wave spectral components (wave translation) over the separation time τ between looks. The deep water dispersion relation for surface gravity waves gives $\omega = (g|\vec{k}|)^{1/2}$. The quasi-linear limit represents a weakly nonlinear approximation to the full nonlinear transform. While it is not strictly valid for RADARSAT ($R/V \sim 120$s), there is some suggestion that its utility may be extended by straightforward modifications to the basic wave-SAR map (e.g. [15], [26]). In any case, we adopt the philosophy that the analytically and numerically much simpler quasi-linear transform is a useful approximation, and in Section 3.2 demonstrate its central role as an intermediary in the inversion of the fully nonlinear transform.

Figure 6 shows the normalized quasi-linear map for an input white wave spectrum ($W(\vec{k}) = 1$) with $\tau = 0$. This approximates the transfer function between the wave and SAR auto-spectra or,

alternatively, the gain window through which the SAR sees the ocean wave spectrum. Its main features are the azimuth cutoff for $|k_a| > 0.05\text{m}^{-1}$, and near zero regions near the origin. The modification for the cross-spectral case ($\tau > 0$) may also be readily ascertained from Figure 6. For our RADARSAT cases, $\tau \sim 0.4$s and we consider the wavenumber domain $|k_a|, |k_r| < 0.15\text{m}^{-1}$. According to (3), the coincident spectrum is just the auto-spectrum multiplied by $\cos(\omega\tau)$. This corresponds to Figure 6 multipled by a factor varying from 1 at the origin, to 0.8 near the edges. Similarly, the quadrature spectrum has a $\sin(\pm\omega\tau)$ in (3); the multiplication factor is zero at the origin and rises to less than $1/2$ the value of the auto-spectrum at the edges. Thus, the coincident spectrum is larger in magnitude and slightly biased towards low wavenumber information, while the quadrature spectrum is smaller in magnitude and biased towards higher wavenumber information. This fact, coupled with sampling variability, helps explain the observed RADARSAT cross-spectra of Figures 2 and 4. The nonlinear transform acts to couple the real and imaginary parts.

Practical (numerical) implementation of the wave-SAR transform is carried out in a discrete vector space. The discrete wave-SAR transform may be represented as

$$\mathbf{s}_{nl} = \mathbf{h}\{\mathbf{w}\}, \tag{4}$$

where $\mathbf{w}$ is a vector containing the wave spectrum $W(\vec{k})$ evaluated over a lattice of range and azimuth wavenumbers and vectorized. The nonlinear vector operator $\mathbf{h}\{\cdot\}$ denotes the wave-SAR transform, and $\mathbf{s}_{nl}$ is the predicted SAR (auto- or cross-) spectrum defined over the same wavenumber grid. We assume, without loss of generality, that all quantities in (4) are real valued. (Real and imaginary parts of the complex valued SAR cross-spectrum can be treated as separate elements in $\mathbf{s}_{nl}$. Note also that the regression based development of Section 3.2 may be cast in equivalent terms for either the real or complex case [3]).

The wave-SAR transform is often modified to take account non-wave processes which influence the observed spectrum through changes in the scattering properties of the air-sea interface. For instance, [26] points out the role of wind effects on the scene coherence time and suggests fitting for the azimuth cutoff K_c on a case dependent basis. [20] absorbs wind effects into the real aperture radar modulation transfer functions which underlie the wave-SAR transform. [15] derives a modified wave-SAR transform to account for point target spreading due to finite sensor resolution. Such case dependent modifications to the wave-SAR transform are examined in Section 4.

3.2   Inversion of the Forward Map

The general inverse problem associated with estimating waves from SAR has two main elements: *(i)* a parameter estimation problem associated with determining unknown or poorly specified quantities

such as K_c, and *(ii)* a state estimation problem associated with the recovery of the wave spectrum. Estimation of these unknowns relies on the observed SAR spectra and, where available, prior knowledge on the wave spectrum (e.g. from a wave model). We consider separately the parameter and state estimation problems. Parameter estimation involves compensating for case-specific effects in the wave-SAR transform and it is treated in Section 4. State estimation deals directly with the wave information content of the SAR and is examined in detail below.

The state estimation problem is governed by the following system of regression equations,

$$\mathbf{s} = \mathbf{h}\{\mathbf{w}\} + \mathbf{e}_o, \qquad \mathbf{w}_p = \mathbf{w} + \mathbf{e}_p. \tag{5}$$

The first equation describes the measurement process with $\mathbf{s}$ denoting the observed SAR (auto- or cross-) spectrum and $\mathbf{w}$ the underlying true value of the wave spectrum. The zero-mean measurement error $\mathbf{e}_o$ has covariance $\mathbf{\Sigma}_o$. The second equation accounts for the prior wave estimate $\mathbf{w}_p$ and its zero-mean error is given as $\mathbf{e}_p$ with covariance $\mathbf{\Sigma}_p$. (The assumption of unbiased error could be relaxed). Note that we make use of a *wide sense* (*WS*) assumption about the error processes wherein no distributional assumptions are made excepting the specification of the first and second moments.

Recovering a minimum variance estimate[1] for the underlying true wave spectrum from (5) leads to the minimization of a cost function,

$$
\begin{aligned}
J &= [\mathbf{s} - \mathbf{h}\{\mathbf{w}\}]^T \mathbf{\Sigma}_o^{-1} [\mathbf{s} - \mathbf{h}\{\mathbf{w}\}] + [\mathbf{w}_p - \mathbf{w}]^T \mathbf{\Sigma}_p^{-1} [\mathbf{w}_p - \mathbf{w}] \\
&= \|\mathbf{s} - \mathbf{h}\{\mathbf{w}\}\|^2_{\mathbf{\Sigma}_o^{-1}} + \|\mathbf{w}_p - \mathbf{w}\|^2_{\mathbf{\Sigma}_p^{-1}}
\end{aligned}
\tag{6}
$$

with respect to $\mathbf{w}$. The first term in J is the weighted squared observation error, $\mathbf{e}_o^T \mathbf{\Sigma}_o^{-1} \mathbf{e}_o$, and represents both non-wave noise processes in the SAR spectrum as well as model errors in the wave-SAR transform. The second term is the weighted squared error of the prior wave estimate, $\mathbf{e}_p^T \mathbf{\Sigma}_p^{-1} \mathbf{e}_p$, and represents deviations of this prior from the underlying true wave spectrum.

The general form of the cost function (6) is applicable to nearly all wave-SAR studies. Additional terms may be included in J to control properties of integral features such as the significant wave height or mean propagation direction [12]. This corresponds to adding further prior information and can be absorbed into this general framework. It is notable that the weighting functions (the inverse error covariances $\mathbf{\Sigma}_o^{-1}, \mathbf{\Sigma}_p^{-1}$) used in the cost function often vary a great deal between studies (contrast [15], [8], and [12]). The consequence of these differences in the quantity to be minimized is

---

[1] Maximum likelihood estimates would require considering the probability density functions of $\mathbf{e}_o$ and $\mathbf{e}_p$. However it is notable that under a wide variety of distributional assumptions, practical implementation of nonlinear regression leads to use of generalized (or iteratively re-weighted) least-squares estimators, e.g. [3], [23].

an improper accounting for the relative role of SAR derived and prior wave information for different regions of the wavenumber domain. This leads to practical difficulties in comparing methods and their results. We demonstrate below that the final estimates of the state and its error variance, as well as the convergence of the minimization procedure, are strongly influenced by choice of $\mathbf{\Sigma}_o$ and $\mathbf{\Sigma}_p$.

In nonlinear wave-SAR inversion, minimization of the cost function is generally carried out iteratively based on an incremental updating of a first guess wave spectrum (e.g. [10]). Denote $\mathbf{w}_n$ as the estimate of the wave spectrum at iteration n of the minimization procedure. The updated wave spectrum takes the form

$$\mathbf{w}_{n+1} = \mathbf{w}_n + \delta\mathbf{w} \tag{7}$$

where $\delta\mathbf{w}$ denotes the incremental change to the current estimate of the wave spectrum. Substituting this in the cost function (6) yields, for the nth iteration,

$$J_n = \|\mathbf{s} - \mathbf{h}\{\mathbf{w}_n + \delta\mathbf{w}\}\|^2_{\mathbf{\Sigma}_o^{-1}} + \|\mathbf{w}_p - (\mathbf{w}_n + \delta\mathbf{w})\|^2_{\mathbf{\Sigma}_p^{-1}} . \tag{8}$$

Taking the leading order term of a Taylor expansion of $\mathbf{h}\{\mathbf{w}_n + \delta\mathbf{w}\}$ about $\mathbf{w}_n$ allows (8) to be written

$$J_n = \|\delta\mathbf{s} - \mathbf{H}\delta\mathbf{w})\|^2_{\mathbf{\Sigma}_o^{-1}} + \|\delta\mathbf{w}_p - \delta\mathbf{w}\|^2_{\mathbf{\Sigma}_p^{-1}} . \tag{9}$$

where the increments are defined as: $\delta\mathbf{s} = \mathbf{s} - \mathbf{h}(\mathbf{w}_n)$, $\delta\mathbf{w}_p = \mathbf{w}_p - \mathbf{w}_n$, and $\delta\mathbf{w} = \mathbf{w} - \mathbf{w}_n$. The wave-SAR transform linearized about the current state is $\mathbf{H} = (\partial\mathbf{h}/\partial\mathbf{w})_{\mathbf{w}=\mathbf{w}_n}$. Each iteration then requires the minimization of a quadratic cost function; the full solution is a sequence of linear estimation problems. Statistically, the above represents an extension of the Gauss-Newton method of nonlinear regression (e.g. [23]) to the random-β case (Appendix B).

Within each iteration of the multi-step minimization of the cost function (6), a linear regression problem must be solved. This yields the incremental change in the wave spectrum at iteration n, i.e.

$$\hat{\delta\mathbf{w}} = \mathbf{\Sigma}_w \left(\mathbf{H}^T \mathbf{\Sigma}_o^{-1} \delta\mathbf{s} + \mathbf{\Sigma}_p^{-1} \delta\mathbf{w}_p \right) \tag{10}$$

with

$$\mathbf{\Sigma}_w = \left(\mathbf{\Sigma}_p^{-1} + \mathbf{H}^T \mathbf{\Sigma}_o^{-1} \mathbf{H} \right)^{-1} . \tag{11}$$

Here, $\mathbf{\Sigma}_w$ provides an asymptotic estimate for the error covariance of the predicted wave spectrum (Appendix B).

The general development presented here makes clear that three quantities play a key role in wave-SAR inversion: $\mathbf{\Sigma}_p$, $\mathbf{\Sigma}_o$, and $\mathbf{H}$. As remarked upon previously, $\mathbf{\Sigma}_o$ and $\mathbf{\Sigma}_p$ influence the choice of the quantity to be minimized, the convergence path taken, and the validity of the final wave

estimates and associated errors. Consider now the specification of the quantity $\mathbf{H}$, the linearization of the wave-SAR map about the current wave state. [8] offers an analytic gradient expression $\partial J / \partial \mathbf{w}$ for a simplified version of (6) in which an exact linearization of the wave-SAR map is implicit. However, a common strategy, motivated by the complexity of the nonlinear transform and its differentiation, is to approximate $\partial \mathbf{h} / \partial \mathbf{w}$ by an iteration invariant $\mathbf{H}$ derived from the quasi-linear transform (e.g. [15], [12]). Since J in (6) remains defined in terms of the full nonlinear transform $\mathbf{h}\{\mathbf{w}\}$, the consequence of using an approximate $\mathbf{H}$ rests only in the convergence properties of the algorithm. This is briefly illustrated below.

To examine the convergence of the minimization procedure, suppose that we have an estimate $\mathbf{w}_n$ and seek an update of the form (7) based on the increment (10). If $\mathbf{w}_n$ is sufficiently close to its true value $\mathbf{w}_t$, we may carry out a Taylor expansion of $\mathbf{h}\{\mathbf{w}_n\}$ about $\mathbf{w}_t$. This leads to the following convergence formula, valid in the vicinity of the true minimum,

$$[\mathbf{w}_{n+1} - \mathbf{w}_t] = \mathbf{A}\,[\mathbf{w}_n - \mathbf{w}_t] \tag{12}$$

where

$$\mathbf{A} = \mathbf{I} - \mathbf{\Sigma}_w \left(\mathbf{H}^T \mathbf{\Sigma}_o^{-1} \left. \frac{\partial \mathbf{h}}{\partial \mathbf{w}} \right|_{\mathbf{w}=\mathbf{w}_t} + \mathbf{\Sigma}_p^{-1} \right).$$

with $\mathbf{I}$ denoting the identity matrix. If the eigenvalues of $\mathbf{A}^T\mathbf{A}$ are less than one in absolute value, then convergence will be achieved as $n \to \infty$. Note that if $\mathbf{H} = \partial \mathbf{h} / \partial \mathbf{w}|_{\mathbf{w}=\mathbf{w}_t}$ convergence is achieved immediately. Otherwise, it is the 'closeness' of an approximate $\mathbf{H}$ to $\partial \mathbf{h} / \partial \mathbf{w}|_{\mathbf{w}=\mathbf{w}_t}$ (in terms of the eigenvalues of $\mathbf{A}^T\mathbf{A}$) that will dictate the convergence properties. Numerous wave-SAR studies suggest (but do not prove) that the quasi-linear transform provides a reasonable approximation to an exact linearization and that convergence can be achieved under a variety of circumstances (e.g. [15], [12]). However, the exact gradient of [8] does have attractive theoretical properties and deserves further examination.

3.3   Limiting Cases

Case 1: SAR only

Consider the situation where wave estimation must rely on SAR alone. Observability is the main issue in the sense that there are wavenumber regions where SAR provides no wave information. These null spaces are evident in Figure 6. For a linearized wave-SAR map, the regression $\mathbf{s} = \mathbf{H}\mathbf{w} + \mathbf{e}_o$ with solution $\hat{\mathbf{w}} = (\mathbf{H}^T\mathbf{\Sigma}_o^{-1}\mathbf{H})^{-1}\mathbf{H}^T\mathbf{\Sigma}_o^{-1}\mathbf{s}$ cannot be achieved directly. Singular value decomposition offers one solution for such rank-deficient regression problems (e.g. [2]). However, it relies on an implied prior based on a minimum norm for the solution vector $\hat{\mathbf{w}}$; this effectively sets

wave estimates in spectral null spaces to zero. The implication for the nonlinear inversion is that portions of a first guess wave which project into the null space will not be changed in subsequent iterations (the algorithm may converge, but the inverse problem effectively remains ill-posed). The first guess wave acts as a prior estimate for that portion of the wave spectrum not observable by the SAR.

Case 2: Blending of SAR and Prior Wave Information

Consider the linearized wave-SAR transform as above. If $\mathbf{H}$ is a diagonal matrix, SAR derived wave estimates for the ith wavenumber bin are determined as $w_{sar} = \mathbf{H}_{ii}^{-1}\mathbf{s}_i$ (where $\mathbf{H}_{ii}^{-1}$ exists). Furthermore, assume that w_p is the ith element of $\mathbf{w}_p$, and that $\mathbf{\Sigma}_o \sim WS(0, \sigma_o^2\mathbf{I})$ and $\mathbf{\Sigma}_p \sim WS(0, \sigma_p^2\mathbf{I})$. For each admissible wavenumber bin i, the wave estimate $\hat{w}$ takes the form,

$$\hat{w} = \left(\frac{1}{1+\gamma}\right) w_{sar} + \left(\frac{1}{1+\gamma^{-1}}\right) w_p.$$

where $\gamma = \mathbf{H}_{ii}^{-2}\sigma_o^2/\sigma_p^2$. The final wave estimate is simply a weighted sum of the SAR-derived and the prior wave estimates. The weighting is governed by γ which may be interpreted as the ratio of *(i)* the error variance of SAR observations scaled by the inverse transform, to *(ii)* the error variance of the prior wave estimate. If $\gamma \gg 1$, such as might be expected in wavenumber regions corresponding to null spaces of the transform, the estimate reverts to w_p. If $\gamma \ll 1$, the estimate becomes w_{sar}.

4 Application

In this section, we examine some practical aspects of the wave-SAR inverse problem using the observed SAR image cross-spectra. This is carried out in the context of the statistical estimation procedure of the previous section and makes use of a modified quasi-linear wave-SAR transform which includes case-specific non-wave geophysical and imaging effects. (Note that use of the non-linear transform did not appear justified on the basis of its ability to explain additional variability found in the observed SAR spectra).

The observed RADARSAT SAR image cross-spectra contain features not accounted for by the basic wave-SAR transform of Appendix A. These include broadband noise due to residual speckle, spectral falloff at higher wavenumbers due to finite sensor resolution, and geophysical (e.g. wind) modifications to the azimuth cutoff. While some progress has been made in understanding these processes, in practice they tend to be addressed either through standard pre-processing procedures [17], or through fitting exercises based on observed SAR auto-spectra (e.g. [26], [15]). As an alternative procedure, we consider SAR image cross-spectra and a parameter estimation procedure

which takes account of prior wave information in order to modify the basic wave-SAR transform. Below, we consider the coincident spectra in detail and use the quadrature spectra only for its phase information.

In order to modify the wave-SAR map for case-specific effects, we seek to minimize a discrete version of the cost function

$$J_s = \int \left| S_{obs}(\vec{k}) - S_{mod}(\vec{k}) \right|^2 d\vec{k}$$

where S_{obs} and S_{mod} denote the observed and modelled SAR coincident spectra, respectively. We assume the following form for S_{mod},

$$S_{mod}(\vec{k}) = \Gamma_{mod}(\vec{k}) \times \left(c_n + \Re\{S_{ql}(\vec{k})\} \right). \tag{13}$$

Here, $\Gamma_{mod}(\vec{k}) = \exp\left\{ -(c_r k_r^2 + c_a k_a^2) \right\}$ with c_r and c_a representing the falloff in power in the azimuth and range directions. This falloff is due to point target spreading and, in the case of c_a, wind effects on the azimuth cutoff. c_n represents a speckle based noise floor and is strictly valid only for i.i.d. speckle [9]. The real part of the wave-SAR map $\Re\{S_{ql}(\vec{k})\}$ is based on (3) using $W(\vec{k})$ from the observed buoy wave spectra. The radar modulation transfer functions in $S_{ql}(\vec{k})$ follow [17] with the parameters of Table 1. The unknown parameters c_n, c_a, and c_r were estimated using a simplex method for nonlinear minimization [21]. Results are given in Table 2. Note that while the predicted azimuth cutoff factor $\rho_{AA}(0)$ (derived from the basic wave-SAR transform) is quite variable, allowing for inclusion of a case-specific c_a has rendered the cutoff wavenumber K_c more stable and realistic.

Simulated SAR coincident spectra were calculated using the modified wave-SAR transform and the estimated values of c_n, c_a, and c_r from Table 2 (see Figure 7). The simulated SAR spectra compare reasonably well with the observed spectra of Figure 2 (correlations are given in Table 2). Cases 1-3 show good correspondence in terms of both the overall magnitudes, peak locations and level of the broadband noise. In cases 4 and 5 the observed and modelled SAR spectra compare less well. This results from peaks in the observed wave and SAR spectra being offset across the zero range and zero azimuth wavenumber axes, respectively (compare Figures 1 and 2). Case 6 shows a situation where the modified transform predicts range splitting where none is found.

The observation error structure was next determined based on analysis of the residuals $e(\vec{k}) = S_{obs}(\vec{k}) - S_{mod}(\vec{k})$ between the observed and predicted SAR coincident spectra. The postulated error variance structure follows (13) and takes the form,

$$\sqrt{\text{var}\{e(\vec{k})\}} = \Gamma_{err}(\vec{k}) \times \left(\sigma_n + \sigma_m \phi(\vec{k}) \right). \tag{14}$$

The Gaussian function $\Gamma_{err}(\vec{k})$ captures the falloff in the magnitude of the error with increasing wavenumber, σ_n is a wavenumber independent noise term, and the model error term consists of

scaling factor σ_m multipled by the structure function $\phi(\vec{k})$. For simplicity, $\phi(\vec{k})$ is taken to be the quasi-linear wave-SAR map with an input white wave spectrum (see Figure 6) and modified to use the cutoff wavenumber K_c from Table 2. Residual analysis suggests a case-independent estimate for Γ_{err} (with energy falloff factors $c_r = 100$ and $c_a = 200$) and for the noise level ($\sigma_n = 1$). The case dependent σ_m had the following values: 1.5, 2.1, 2.3, 10.5, 1.9, and 9.8 for cases 1-6 respectively. The high values in cases 4 and 6 resulted from mismatches in the spectral distribution of energy in the observed SAR and buoy wave spectra. Error correlations are assumed isotropic in wavenumber and based on the smoothing kernel applied to the raw SAR spectra. Figure 8 shows the error variance for case 1. The above error analysis allows us to specify $\mathbf{\Sigma}_o$.

As a pre-processing step in wave-SAR inversion, we separate the wave signal from non-wave processes to avoid any broad-band noise present in the observed SAR being attributed to ocean wave energy. First, regions of the coincident spectra were identified corresponding to coherency greater than 0.6 (see Section 2). Second, the corresponding mean phase values in each of these coherent regions are used to identify the portion of the SAR spectrum corresponding to the wave propagation direction (see Figure 5). Finally, a noise floor is subtracted from these spectral regions whose magnitude is based on the results given in Table 2. This procedure identifies the portion of the observed SAR spectrum with useful wave information.

Figure 9 shows SAR-derived wave estimates based on inversion of the wave-SAR transform. These are based on the coherency and phase filtered SAR spectrum, $\mathbf{s}$, and the modified wave-SAR transform, $\mathbf{H}$, of (13) using the values of Table 2 but with $c_n = 0$ (we have removed the noise floor). Wave estimates are then determined as $\hat{\mathbf{w}} = (\mathbf{H}^T \mathbf{\Sigma}_o^{-1} \mathbf{H})^{-1} \mathbf{H}^T \mathbf{\Sigma}_o^{-1} \mathbf{s}$. Null spaces where the SAR has no information content are explicity identified as part of this inversion procedure. It is clear that comparison of the SAR derived wave estimates with the buoy spectra would normally take place in a very limited region of the wavenumber plane. Moreover, the information content of these non-null regions must take account of the error variance of the SAR derived wave. Panel (b) of Figure 8 shows this error variance for case 1. Note that in spectral regions adjacent to null spaces the error variance tends to be large reflecting the sensitivity of wave estimates to the azimuth cutoff. The overall energy content of the SAR derived and buoy wave spectra in non-null regions show a reasonable match in all cases with the exception of cases 4 and 6.

Estimation of the complete directional wave spectrum must combine wave information from the (band limited) SAR with the (broad band) buoy wave spectra, taking into account the wavenumber dependence of their respective error covariances. Initial experiments with direct blending of the SAR and buoy information using (10) lead to discontinuties near the azimuth cutoff (imagine combining the wave spectra in Figures 1 and 9, also see Section 3.3). However, the error variance of the wave

estimates (panel (c) of Figure 8) reveals the main properties associated with the blending of SAR and prior wave estimates: null spaces are eliminated and the overall error variance is reduced.

As an alternative to direct blending, we also considered parameterization of the true wave spectrum in terms of the buoy spectrum, but allow for its free rotation through an angle θ. In terms of the cost function (6), or (9), we let $\mathbf{w} = \mathrm{rot}\{\theta; \mathbf{w}_p\}$ and we minimize J with respect to θ. The two terms in the cost function are then interpreted as measuring the weighted squared differences between: *(i)* the observed SAR spectrum and that predicted using the rotated buoy wave spectrum, and *(ii)* the buoy wave spectrum and its rotated version. The second term acts as a regularization term that biases the final estimator towards a state of minimal rotation. For simplicity we assume $\mathbf{\Sigma}_p = \sigma_p^2 \mathbf{I}$. Figure 10 shows the cost function J versus the rotation angle θ for the 6 cases. Three treatments are applied: baseline ($\sigma_p^{-2} = 0$), weak regularization ($\sigma_p^{-2} = 15^{-2}$), and strong regularization ($\sigma_p^{-2} = 10^{-2}$). The results indicate multiple minima in J for the baseline situation. Strong regularization generally biases results heavily towards $\theta = 0$. Weak regularization allows for an unambiguous choice of the optimal θ required to bring the wave spectra of Figure 1 into agreement with the SAR based wave information. Generalized cross-validation would provide a more formal means to choose the strength of the regularization term [4].

5   Summary and Conclusions

In this paper, we have examined the problem of extracting information on the directional ocean wave spectrum from SAR imagery. A unique aspect of this study is its emphasis on statistical aspects of the inverse problem, as well as the use of SAR image cross-spectra. Our framework for wave-SAR inversion allows the wave information content of SAR to be quantified on a wavenumber dependent basis. The RADARSAT SAR data used here were processed into two looks at the same ocean scene separated by 0.4 seconds. Speckle noise was greatly reduced in comparison with the SAR auto-spectra, though some broad band noise persisted. The coincident spectrum clearly showed the wave modulation of the radar cross-section in limited, but identifiable, regions of wavenumber space. The quadrature spectrum had much greater variability but the associated phase spectrum was able to resolve propagation direction for most cases. However, the mean phase values in each of the wave groups varied significantly about the value expected based on a deep water dispersion relation.

The extraction of wave information from observed SAR spectra was examined from the perspective of a statistical estimation problem, specifically a random-β extension of nonlinear regression (Appendix B). This general formulation highlights key issues and allowing an assessment of the consequences of the differing assumptions made in past wave-SAR inversion work. It was shown

that the wave-SAR inverse problem requires estimates for the error covariances associated with *(i)* the observed SAR (including errors in the wave-SAR transform), and *(ii)* the prior wave estimates. Specification of these quantities varies widely between studies (contrast [12], [15], [8]). Another common simplification of wave-SAR studies uses the the quasi-linear wave-SAR map as an intermediary in the inversion of the fully nonlinear transform (e.g. [10], [12]). We showed how this approximation to an exact linearization of the wave-SAR map about the current wave state is linked to the convergence properties of the minimization algorithm. These are important issues to consider for the use of SAR in a wave data assimilation system.

A simple wave-SAR inversion procedure was carried out for the purpose of examining practical issues pertinent to wave extraction from SAR. Towards this end, we elected to focus on the real part of the SAR image cross spectra, and use the quadrature spectra only for its phase information. A modified wave-SAR transform was used that empirically accounted for broad-band residual speckle [9], spectral falloff with increasing wavenumber [17], [15] and sea surface effects on the azimuth cutoff [26]. These parameters were estimated using a fitting procedure designed to minimize the squared difference between the observed and modelled SAR coninicident spectra. A canonical form for the observation error covariance was determined based on an analysis of the residuals between the observed and predicted SAR coincident spectra. Wave extraction from the SAR spectra was achieved by filtering for broad band noise and wave propagation direction using the coherency and phase spectra. Inversion of the modifed wave-SAR transform emphasized the highly band limited nature of the SAR wave information, and provided for explicit treatment of the null spaces and estimates of the wavenumber dependent error variance.

There are a number of outstanding issues involved in SAR processing for optimal extraction of ocean wave information (e.g. [27]). At the heart of the cross-spectral method is the multi-look processing of the SAR data which produces independent looks at the same ocean scene. Ideally, these looks should be temporally separated by a significant fraction of the period of the dominant wave groups. However, time separations are constrained by the Doppler bandwidth of the SAR to be a fraction of a second. The relation of the noise processes to the Doppler filtering and multi-look processing remains unclear. We also illustrated how the coincident and quadrature spectra provide complementary information on the wave spectra due to the (deep water) dispersion relation embedded in the wave-SAR transform. However, the extent to which look separation and cross-spectral SAR processing may be optimized for the extraction of waves remains an open question.

A key issue in extracting wave information from SAR is the appropriate use of the highly band limited wave information. Null spaces must be explicitly identified and quantitative estimates of the wavenumber dependent error covariance are necessary. We have argued that the observation

error covariance matrix $\boldsymbol{\Sigma}_o$ plays an important role in wave-SAR inversion. This quantity includes shortcomings in the wave-SAR transform, noise and non-wave signals, as well as errors of representativeness due to sampling variability [16]. Our prototype expression for the $\boldsymbol{\Sigma}_o$ reflected two main features: *(i)* compensation for the non-uniform response of the SAR to changes in wave energy for different spectral regions (see [15]), and *(ii)* uncertainties associated with noise and pre-processing. Our treatment has taken account of the full wavenumber plane and emphasizes that the SAR provides as much information about both where the wave energy is located in wavenumber space, as well as regions in which there is no wave energy. This treatment would be greatly enhanced by a more extensive data set on which to base the error analysis.

The assimilation of SAR in operational wave models is under active development [6]. Like many satellite data sources, SAR is nonlinearly related to the prognostic variables of interest (i.e. a nonlinear measurement operator). We have outlined the estimation problem associated with the use of SAR in a wave data assimilation context. Blending of the band limited SAR derived waves with model estimates requires additional assumptions in order to obtain physically realizable wavenumber spectra (e.g. to account for spectral discontinuties near the azimuth cutoff). Unfortunately generic spectral shapes for swell do not exist, unlike for a wind sea [19]. Parameterization of the wave-spectral shape in terms of that predicted by a wave model has been suggested [12]. Our simple experiments with such a parameterization, allowing for free rotation of the spectral shape, indicated the complexity of such an optimization: multiple minima were found in the cost function and additional regularization was required.

In conclusion, satellite-based SAR inter-look image cross spectra offers useful, though limited, information on the directional ocean wave spectrum. A basic understanding of the inverse problem associated with wave extraction from SAR is central to the continued use of SAR for understanding ocean waves. We have examined a regression based framework to investigate the problem and emphasize the importance of taking proper account of uncertainities in the observed SAR spectrum and the wave-SAR transform. Continued investigation of SAR imagery co-located with *in situ* wave information is needed (e.g. [20]). These studies should focus on rectifying uncertainties in the wave-SAR transform, as well as providing for a robust statistical description of non-wave, geophysical effects (such as wind) on the SAR spectrum and including parameterization of errors. Such studies would clearly advance the practical use and theoretical understanding of SAR imaging of ocean waves.

Appendix A: The Wave-SAR Transform

The closed form, nonlinear integral transform relating the ocean wave spectrum to the SAR image auto-spectrum is due to [10], and has been extended to the case of SAR image cross-spectra [8]. Following [8], the wave-SAR transform may be summarized as,

$$S(\vec{k}) = \int e^{-i\vec{k}\cdot\vec{x}} G(\vec{x}, \vec{k}) d\vec{x} \tag{15}$$

where $S(\vec{k})$ represents the SAR image cross-spectrum based on two looks at same ocean scene separated by the time interval τ (the functional dependence on τ is implicit). The vector wavenumber $\vec{k} = (k_x, k_y)$ is in satellite coordinates and denotes the cross-track (range) and along-track (azimuth) wavenumbers, respectively. The corresponding coordinates in the spatial (image) domain are given by $\vec{x} = (x, y)$. A basic version of the (wave spectrum dependent) G-function in the integrand takes the form

$$G(\vec{x}, \vec{k}) = \exp\left\{k_y^2\left(\rho_{AA}(\vec{x}) - \rho_{AA}(\vec{0})\right)\right\} \times$$

$$\left\{1 + \rho_{II}(\vec{x}) + ik_y\left(\rho_{IA}(\vec{x}) - \rho_{AI}(\vec{x})\right) + k_y^2\left(\mu_{IA}(\vec{x}) - \mu_{AI}(\vec{x})\right)\right\} \tag{16}$$

where

$$\mu_{ab}(\vec{x}) = \rho_{ab}(\vec{x}) - \rho_{ab}(\vec{0})$$

with a, b denoting one of I or A. The covariance functions ρ_{ab} in the above take the form

$$\rho_{ab}(\vec{x}) = \frac{1}{(2\pi)^2} \int e^{i\vec{k}\cdot\vec{x}}\left(N_{ab}(\vec{k})W(\vec{k}) + N_{ab}^*(-\vec{k})W(-\vec{k})\right) d\vec{k}$$

where $*$ denotes complex conjugation, $W(\vec{k})$ is the ocean wave spectrum, and

$$N_{ab}(\vec{k}) = \frac{1}{2}T_a(\vec{k})T_b^*(\vec{k})e^{i\omega\tau}.$$

Here, the $T_{a,b}$ are the radar modulation transfer functions which summarize the ensemble properties of the interaction of the radar waves with the sea surface with a, b subscripting denoting either the real aperture radar (RAR) tilt and hydrodynamic modulation T_I, or the velocity bunching modulation T_A. [17] gives a very basic form for these relations,

$$T_I = c\, i\, k_x, \qquad T_A = \frac{R}{V}\omega\left(\frac{k_x}{|\vec{k}|}\sin\alpha + i\cos\alpha\right) \tag{17}$$

where c is a constant, R denotes range (distance from the antenna to the target), V is the platform velocity, and α is the incidence angle. More detailed and realistic RAR modulation transfer functions are available and frequently used, e.g. [20].

The wave-SAR transform (1) is generally evaluated based on series expansion of the exponential term $\exp\{k_y^2 \rho_{AA}(\vec{x})\}$ in (16), i.e.

$$S(\vec{k}) = \exp\left\{-k_y^2 \rho_{AA}(\vec{0})\right\} \times \sum_{n=0}^{\infty} \frac{1}{n!} \times \tag{18}$$

$$\left[k_y^{2n} F\left\{\rho_{AA}^n(\vec{x})(1 + \rho_{II}(\vec{x}))\right\} + k_y^{2n+1} F\left\{\rho_{AA}^n(\vec{x})(\rho_{IA}(\vec{x}) - \rho_{AI}(\vec{x}))\right\} + \right.$$

$$\left. k_y^{2n+2} F\left\{\rho_{AA}^n(\vec{x})(\mu_{IA}(\vec{x})\mu_{AI}(\vec{x}))\right\}\right]$$

where F denotes the Fourier transform operator. The integral in (15) is thus cast as a sequence of readily evaluated Fourier transforms.

The analytic properties of the nonlinear wave-SAR transform for the case of SAR auto-spectra ($\tau = 0$) have been examined by [14]. In the cross-spectral case ($\tau > 0$) a phase shift $e^{i\omega\tau}$ is introduced into the N_{ab} function. This represents a simple wave translation model valid over the $O(1\text{s})$ time separation between the looks. The frequency ω can be based on a dispersion relation, which for deep water takes the form $\omega = (g|\vec{k}|)^{1/2}$.

The quasi-linear limit of (18) contains only those terms in the square brackets which are linear in $W(\vec{k})$, i.e.

$$S(\vec{k}) = \exp\left\{-k_y^2 \rho_{AA}(\vec{0})\right\} \left(\Psi(\vec{k})W(\vec{k})e^{i\omega t} + \Psi(-\vec{k})W(-\vec{k})e^{-i\omega t}\right) \tag{19}$$

where

$$\Psi(\vec{k}) = N_{II}(\vec{k}) + ik_y\left(N_{IA}(\vec{k}) - N_{AI}(\vec{k})\right) + k_y^2 N_{AA}(\vec{k}).$$

This represents a weakly nonlinear approximation to the full nonlinear transform, and is uniformly valid over the wavenumber space. Note that it is analytically and numerically much simpler than either (15) or (18).

Appendix B: Random-β Regression

Consider the system of regression equations

$$\mathbf{s} = \mathbf{Hw} + \mathbf{e}_o, \qquad \mathbf{w}_p = \mathbf{w} + \mathbf{e}_p$$

where the regression coefficients $\mathbf{w}$ are treated as a random variable (hence the designation "random-β"). These can be combined a single regression equation as

$$\left(\begin{array}{c} \mathbf{s} \\ \mathbf{w}_p \end{array} \right) = \left(\begin{array}{c} \mathbf{H} \\ \mathbf{I} \end{array} \right) \mathbf{w} + \left(\begin{array}{c} \mathbf{e}_o \\ \mathbf{e}_p \end{array} \right).$$

Assume that the errors are uncorrelated, i.e.

$$\mathrm{var} \left(\begin{array}{c} \mathbf{e}_o \\ \mathbf{e}_p \end{array} \right) = \left(\begin{array}{cc} \mathbf{\Sigma}_o & 0 \\ 0 & \mathbf{\Sigma}_p \end{array} \right),$$

where $\mathbf{\Sigma}_o$ and $\mathbf{\Sigma}_p$ represents the associated error covariance matrices. The above equation is now in standard regression form, and the generalized least squares solution for $\hat{\mathbf{w}}$ is obtained immediately as

$$
\begin{aligned}
\hat{\mathbf{w}} &= \mathbf{\Sigma}_w \left[(\mathbf{H}^T\ \mathbf{I}) \left(\begin{array}{cc} \mathbf{\Sigma}_o^{-1} & 0 \\ 0 & \mathbf{\Sigma}_p^{-1} \end{array} \right) \right] \left(\begin{array}{c} \mathbf{s} \\ \mathbf{w}_p \end{array} \right) \\
&= \mathbf{\Sigma}_w \mathbf{H}^T \mathbf{\Sigma}_o^{-1} \mathbf{s} + \mathbf{\Sigma}_w \mathbf{\Sigma}_p^{-1} \mathbf{w}_p,
\end{aligned}
\tag{20}
$$

where $\mathbf{\Sigma}_w$ is the error covariance matrix of $\hat{\mathbf{w}}$ and given by

$$
\begin{aligned}
\mathbf{\Sigma}_w &= \left[(\mathbf{H}^T\ \mathbf{I}) \left(\begin{array}{cc} \mathbf{\Sigma}_o^{-1} & 0 \\ 0 & \mathbf{\Sigma}_p^{-1} \end{array} \right) \left(\begin{array}{c} \mathbf{H} \\ \mathbf{I} \end{array} \right) \right]^{-1} \\
&= \left[\mathbf{H}^T \mathbf{\Sigma}_o^{-1} \mathbf{H} + \mathbf{\Sigma}_p^{-1} \right]^{-1}.
\end{aligned}
\tag{21}
$$

An alternative expression may be derived as follows. Substituting (21) into (20) and solving for $\hat{\mathbf{w}}$ yields

$$
\begin{aligned}
\hat{\mathbf{w}} &= \mathbf{w}_p + \mathbf{\Sigma}_w \mathbf{H}^T \mathbf{\Sigma}_o^{-1} (\mathbf{s} - \mathbf{Hw}_p) \\
&= \mathbf{w}_p + \mathbf{K}(\mathbf{s} - \mathbf{Hw}_p),
\end{aligned}
$$

where we have defined the gain matrix $\mathbf{K} = \mathbf{\Sigma}_w \mathbf{H}^T \mathbf{\Sigma}_o^{-1}$. This makes clear how the observations may be viewed in terms of updating the prior estimate and is directly linked to a single-stage transition of the Kalman filter [5].

Acknowledgements

References

[1] W.R. Alpers and C. Bruening, "On the relative importance of motion related contributions to the SAR imaging mechanism of ocean surface waves", *IEEE Transactions on Geoscience and Remote Sensing*, vol. 24, pp. 873-885, 1986.

[2] S. Barnett, *Matrices: Methods and Applications*, Oxford, Claredon Press, 450pp, 1990.

[3] D.R. Brillinger, *Time Series. Data Analysis and Theory*, San Francisco, Holden-Day, 540pp, 1981.

[4] P. Craven and G. Wahba, "Smoothing noisy data with spline functions: Estimating the correct degree of smoothing by the method of generalized cross-validation", *Numer. Math.*, vol. 31, pp. 377-403, 1979.

[5] D.B. Duncan and S.D. Horn, "Linear dynamic recursive estimation from the viewpoint of regression analysis", *Journal of the American Statistical Association*, vol. 67, pp. 815-821, 1972.

[6] E.M. Dunlap, R.B. Olsen, L.J. Wilson, S. De Margerie, and R. Lalbeharry, "The effect of assimilating ERS-1 fast delivery wave data into the North Atlantic WAM model", *Journal of Geophysical Research*, vol. 103, pp. 7901-7915, 1997.

[7] G. Engen, K.A. Høgda and H. Johnsen, "A new method for wind field retrieval from SAR data", Proc. CEOS SAR Workshop, WPP-138, ESTEC 3-6 February 1998.

[8] G. Engen and H. Johnsen, "SAR-ocean wave inversion using image cross-spectra", *IEEE Transactions on Geoscience and Remote Sensing*, vol. 33, pp. 1047-1056, 1995.

[9] A.D. Goldfinger, "Estimation of spectra from speckled images", *IEEE Transactions on Aerospace and Electronic Systems*, vol. 18, pp. 675-681, 1982.

[10] K. Hasselmann and S. Hasselmann, "On the nonlinear mapping of an ocean wave spectrum into a synthetic aperture radar image spectrum and its inversion", *Journal of Geophysical Research*, vol. 90, pp. 10713-10729, 1991.

[11] K. Hasselmann, R.K. Raney, W.J. Plant, W. Alpers, R.A. Shuchman, D.R. Lyzenga, C.L. Rufenach, and M.J. Tucker, "Theory of synthetic aperture radar ocean imaging", *Journal of Geophysical Research*, vol. 90, pp. 4659-4686, 1985.

[12] S. Hasselmann, C. Brüning, K. Hasselmann, and P. Heimbach, "An improved algorithm for the retrieval of ocean wave spectra from synthetic aperture radar image spectra", *Journal of Geophysical Research*, vol. 101, pp. 16615-16629, 1996.

[13] H. Johnsen and G. Engen, "Wave Spectra Retrieval from SAR Data", Proc. CEOS Wind and Wave Validation Workshop, WPP-147, ESTEC 3-5 June 1997.

[14] H.E. Krogstad, "A simple derivation of Hasselmann's nonlinear ocean-synthetic aperture radar transform", *Journal of Geophysical Research*, vol. 97, pp. 2421-2425, 1992.

[15] H.E. Krogstad, O. Samset, and P.W. Vachon, "Generalizations on the non-linear ocean-SAR transform and simplified SAR inversion algorithm", *Atmosphere-Ocean*, vol. 32, pp. 61-82, 1994.

[16] F.M. Monaldo, "The consequences of sampling variability on the estimation of wavenumber and propagation direction from spaceborne SAR image spectra", *IEEE Transactions on Geoscience and Remote Sensing*, vol. 29, pp. 113-119, 1991.

[17] F.M. Monaldo and D.R. Lyzenga. "On the estimation of wave slope- and height- variance spectra from SAR imagery", *IEEE Transactions on Geoscience and Remote Sensing*, vol. 24, pp. 543-550, 1986.

[18] J. Oltman-Shay and R. T. Guza, "A data-adaptive ocean wave directional estimator for pitch and roll type measurements", *Journal of Physical Oceanography*, vol. 14, pp. 1800-1810, 1984.

[19] W.J. Pierson and L. Moskowitz. "A proposed spectral form for fully developed wind seas based on the similarity theory of S.A. Kitaigorodskii", *Journal of Geophysical Research*, vol. 69, pp. 5181-5190, 1964.

[20] W.J. Plant and L.M. Zurk, "Dominant wave directions and significant wave heights from synthetic aperture radar imagery of the ocean", *Journal of Geophysical Research*, vol. 102, pp. 3473-3482, 1997.

[21] W.H. Press, S.A. Teukolsky, W.T. Vetterling, and B.P. Flannery, *Numerical Recipes in FOR-TRAN*, New York, Cambridge University Press, 964pp, 1992.

[22] M.B. Priestley, *Spectral Analysis and Time Series*, London, Academic Press, 890pp, 1981.

[23] G.A.R. Seber and C.J. Wild, *Nonlinear Regression*, New York, Wiley, 768pp, 1989.

[24] P.W. Vachon, J.W.M. Campbell, F.W. Dobson, and M.T. Rey, "Ship detection by RADARSAT SAR: Validation of the detection model predictions", *Canadian Journal of Remote Sensing*, vol. 23, pp. 48-59, 1997.

[25] P.W. Vachon and F.W. Dobson, "Validation of wind vector retrieval from ERS-1 SAR images over the ocean", *The Global Ocean and Atmoshere System*, vol. 5, pp. 177-187, 1996.

[26] P.W. Vachon, H.E. Krogstad, and J.S. Paterson, "Airborne and spaceborne synthetic aperture radar observations of ocean waves", *Atmosphere-Ocean*, vol. 32, pp. 83-112, 1994.

[27] P.W. Vachon and J.C. West, "Spectral estimation techniques for multilook SAR images of ocean waves", *IEEE Transactions on Geoscience and Remote Sensing*, vol. 30, pp. 568-577, 1992.

[28] P.W. Vachon and R. K. Raney, "Resolution of the ocean wave propagation direction in SAR imagery", *IEEE Transactions on Geoscience and Remote Sensing*, vol. 29, pp. 105-112, 1991.

Table 1: Summary of the RADARSAT SAR parameters and environmental conditions during MASDE. Satellite parameters include the beam mode, incidence angle α, and the range to velocity ratio R/V. Environmental parameters include: the significant wave height H_s, the peak period T_0, the peak wavenumber k_{peak}, the wind speed at 10m U_{10}, and the wind direction U_{dir} in satellite coordinates with 0° denoting the azimuth direction.

Case	Date	Beam	α	R/V	H_s	T_0	k_{peak}	U_{10}	U_{dir}
1	96/03/20	S3	32.9	123	1.94	4.8	0.04	11.2	257.4
2	96/03/23	W1	25.7	116	1.88	6.3	0.021	6.9	282.6
3	96/03/27	S4	37.6	129	1.17	5.4	0.059	4.9	198.6
4	96/04/03	W3	42.0	137	3.15	5.9	0.008	11.9	118.9
5	96/04/06	S3	27.6	117	0.95	5.3	0.019	5.7	196.1
6	96/04/09	W1	31.2	121	3.67	7.1	0.043	1.5	176.2

Table 2: Characterization of the RADARSAT SAR spectra and the wave-SAR transform. Here, $\rho_{AA}(0)$ is the calculated zero lag of the velocity bunching covariance function (see Appendix A). Estimated azimuth falloff, range falloff, and noise level parameters of the SAR co-spectra are denoted by c_r, c_a, and c_n respectively. K_c is a fitted equivalent rectangular width cutoff wavenumber in m^{-1} (see text). The final column is the correlation between the observed and simulated SAR coincident spectra.

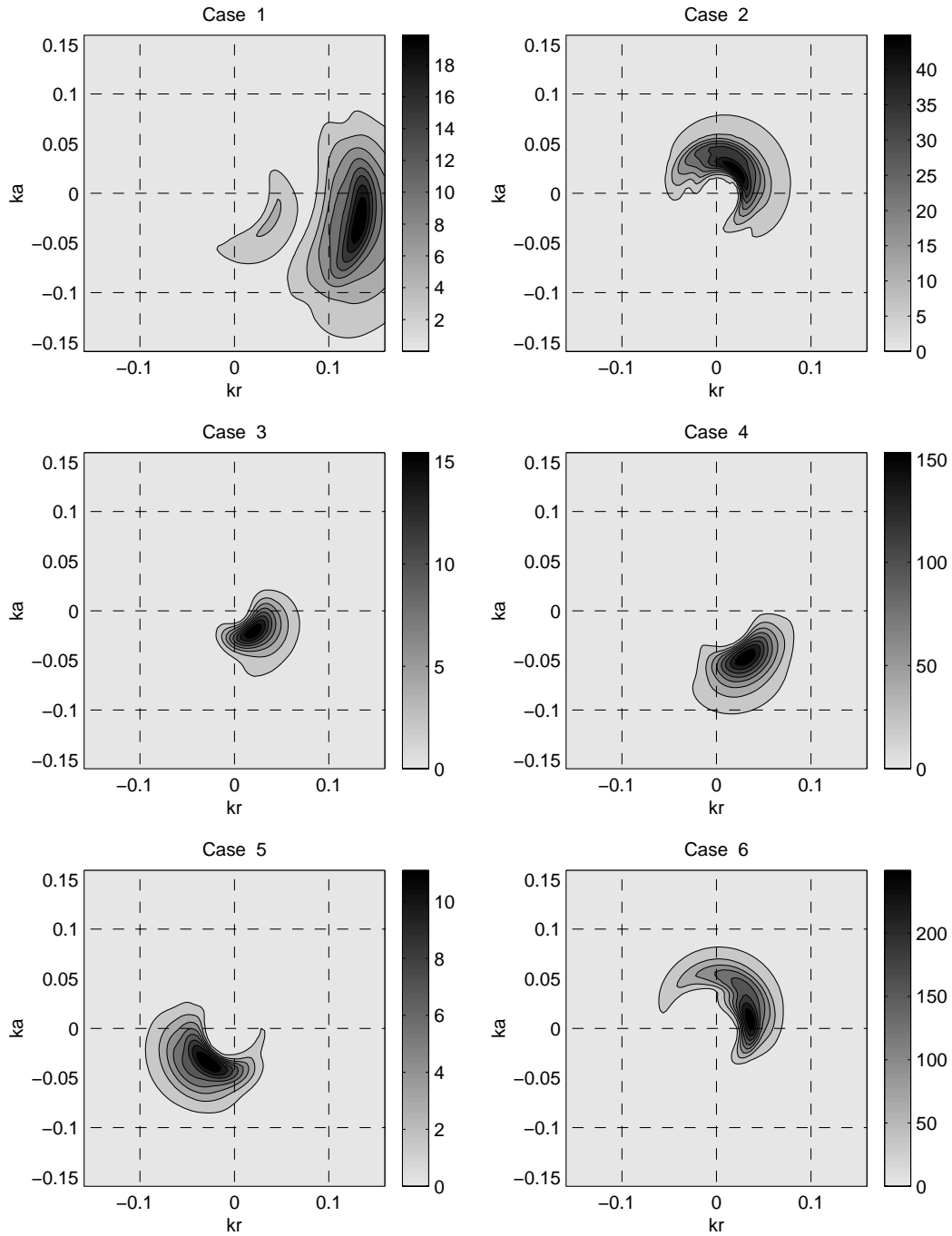| case	$\rho_{AA}(0)$	c_a	c_r	c_n	K_c	corr
1	4825	495.4	132.1	3.665	$2.43(10^{-2})$	0.95
2	1571	2085	176.9	1.687	$2.93(10^{-2})$	0.89
3	200.1	3269	41.62	1.223	$3.01(10^{-2})$	0.79
4	4618	603.2	45.18	0.738	$2.45(10^{-2})$	0.54
5	448.5	940.7	1445.7	1.477	$4.76(10^{-2})$	0.68
6	6541.2	51.90	200.7	1.428	$2.19(10^{-2})$	0.83

Figure 1: Directional wave spectra collected during MASDE from a wave buoy located at 44.5°N, 63°W. These are in satellite coordinates with the axes corresponding to the range 'kr' (cross-track) and azimuth 'ka' (along-track) wavenumbers in radians m^{-1}. The grayscale denotes the spectral density of wave height in m.
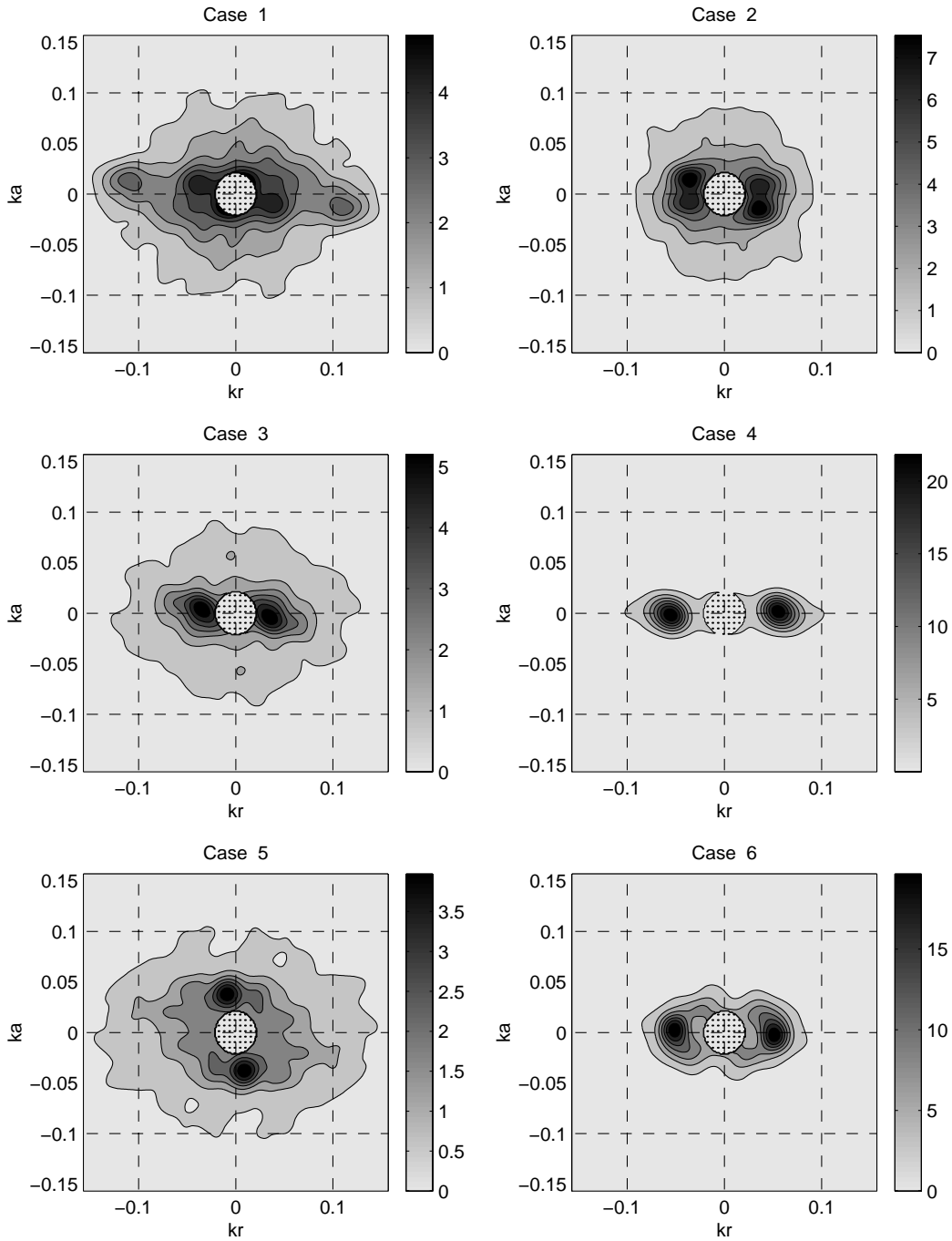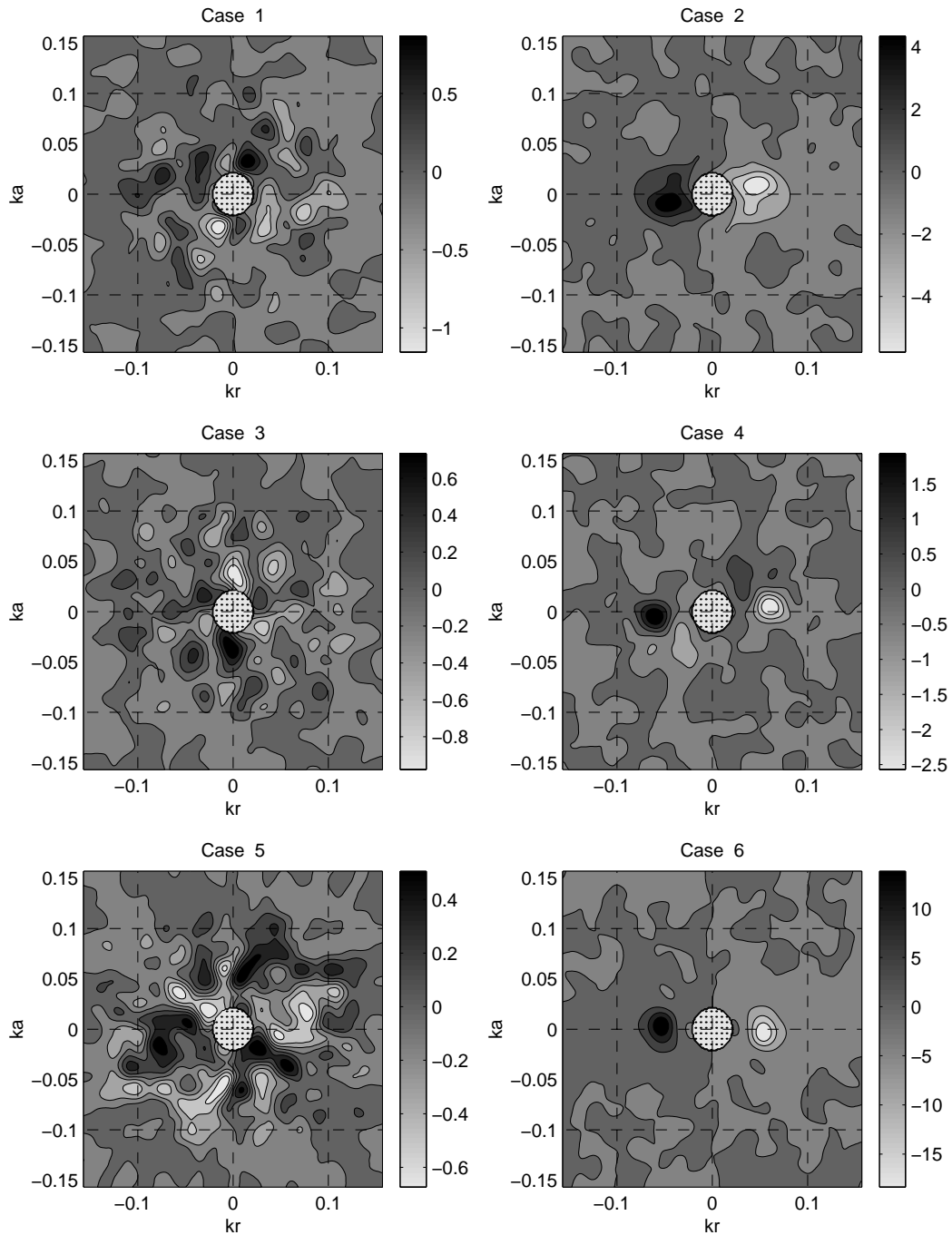
Figure 2: Real part of the RADARSAT SAR image cross spectra derived from 2 looks at the same ocean scene, separated by 0.4s in time. The axes follow Figure 1. The grayscale corresponds to spectral density of the normalized radar cross-section. Note that the region $|\vec{k}| < 2\pi/300$m is marked with dots to emphasize the lack of reliable ocean wave information here.
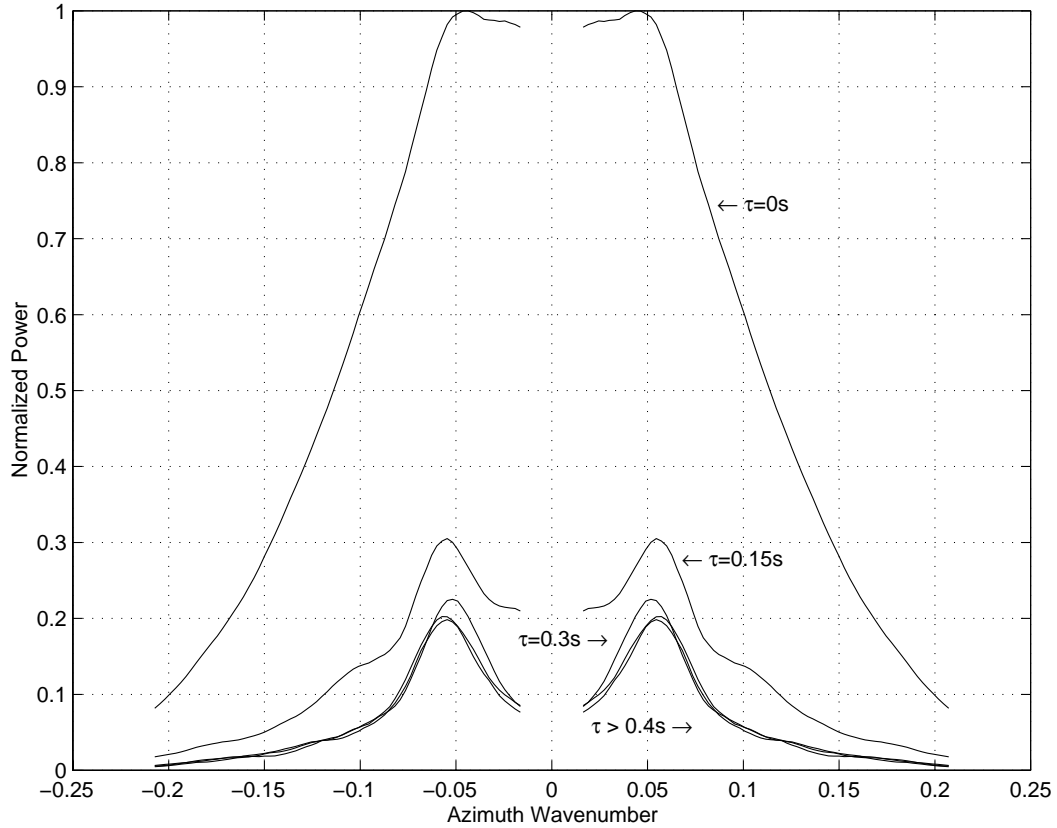
Figure 3: Range-integrated SAR coincident spectra from case 5. The image was re-processed into 5 looks, each with an time separation $\tau \approx 0.15$s. The various curves denote the spectra for the different time separations as indicated. All spectra are normalized by the maximum value of the auto-spectra. Following Figure 2, the region $|k_a| < 2\pi/300$m is left blank.

Figure 4: Imaginary part of RADARSAT SAR image cross spectra derived from 2 looks at the same ocean scene, separated by 0.4s in time. The axes follow Figure 1. The grayscale corresponds to spectral density of the normalized radar cross-section. The dotted area follows Figure 2.
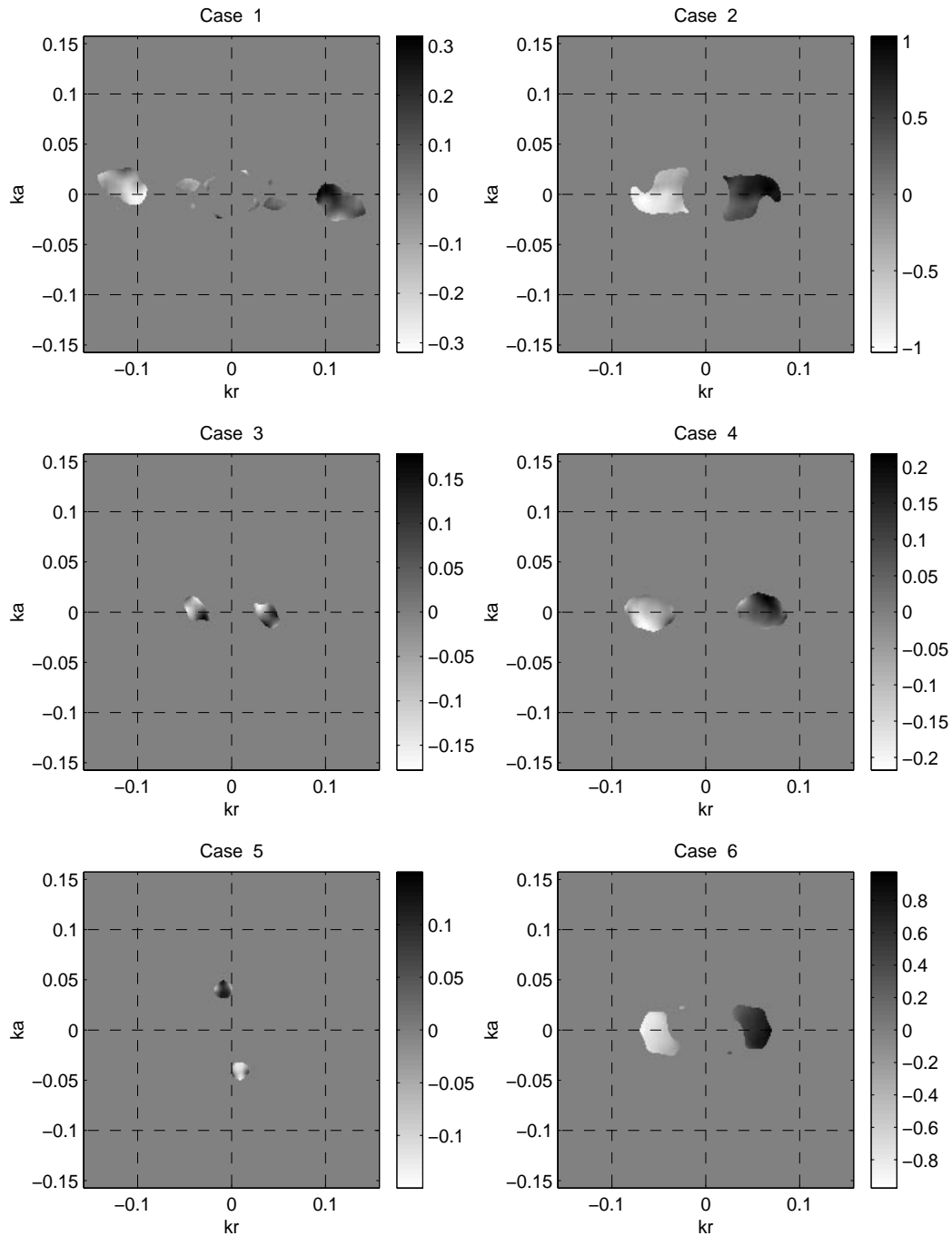
Figure 5: Phase spectra for RADARSAT SAR. For plotting purposes, regions of the phase spectrum having a coherency < 0.6 have been set equal to zero (see text). The axes follow Figure 1. The grayscale indicates the phase in radians.
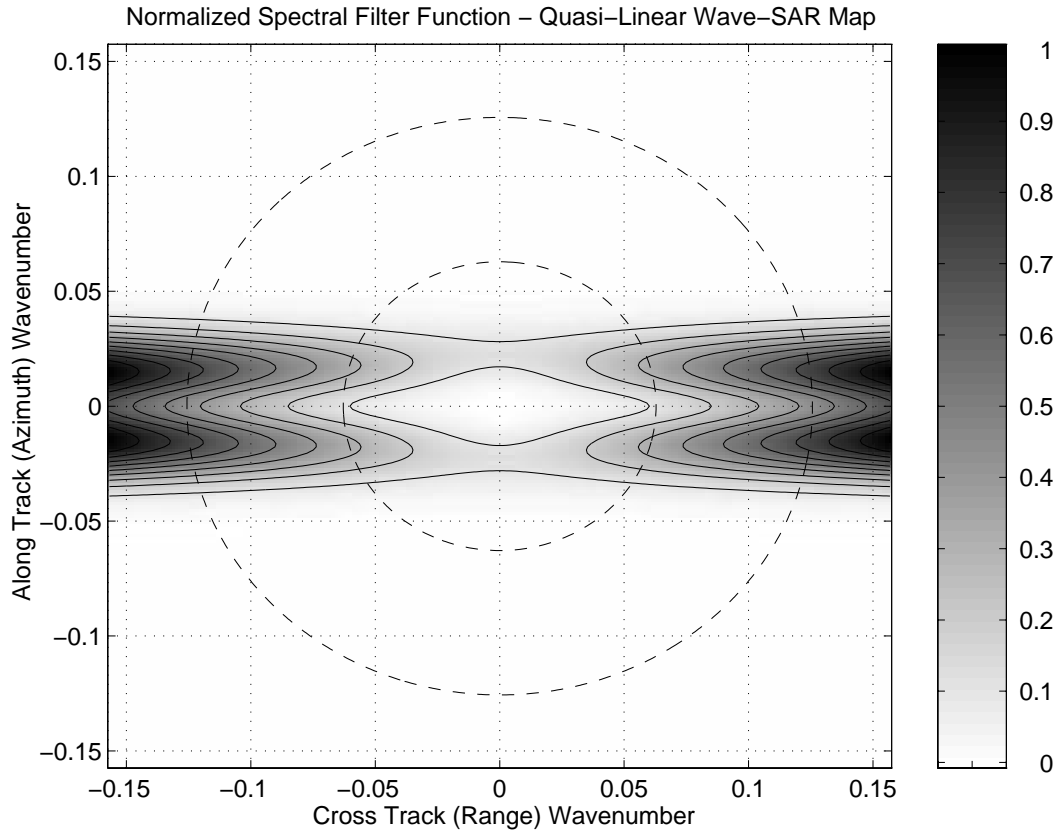
Figure 6: Gain spectrum associated with the basic quasi-linear wave to SAR transform (see Appendix A). This is based on RADARSAT SAR parameters of Table 1 and assumes an input white wave spectrum with $\tau = 0$. An azimuth cutoff wavelength of 125m has been chosen as typical for RADARSAT. The grayscale corresponds to normalized power spectral density of the radar cross-section.
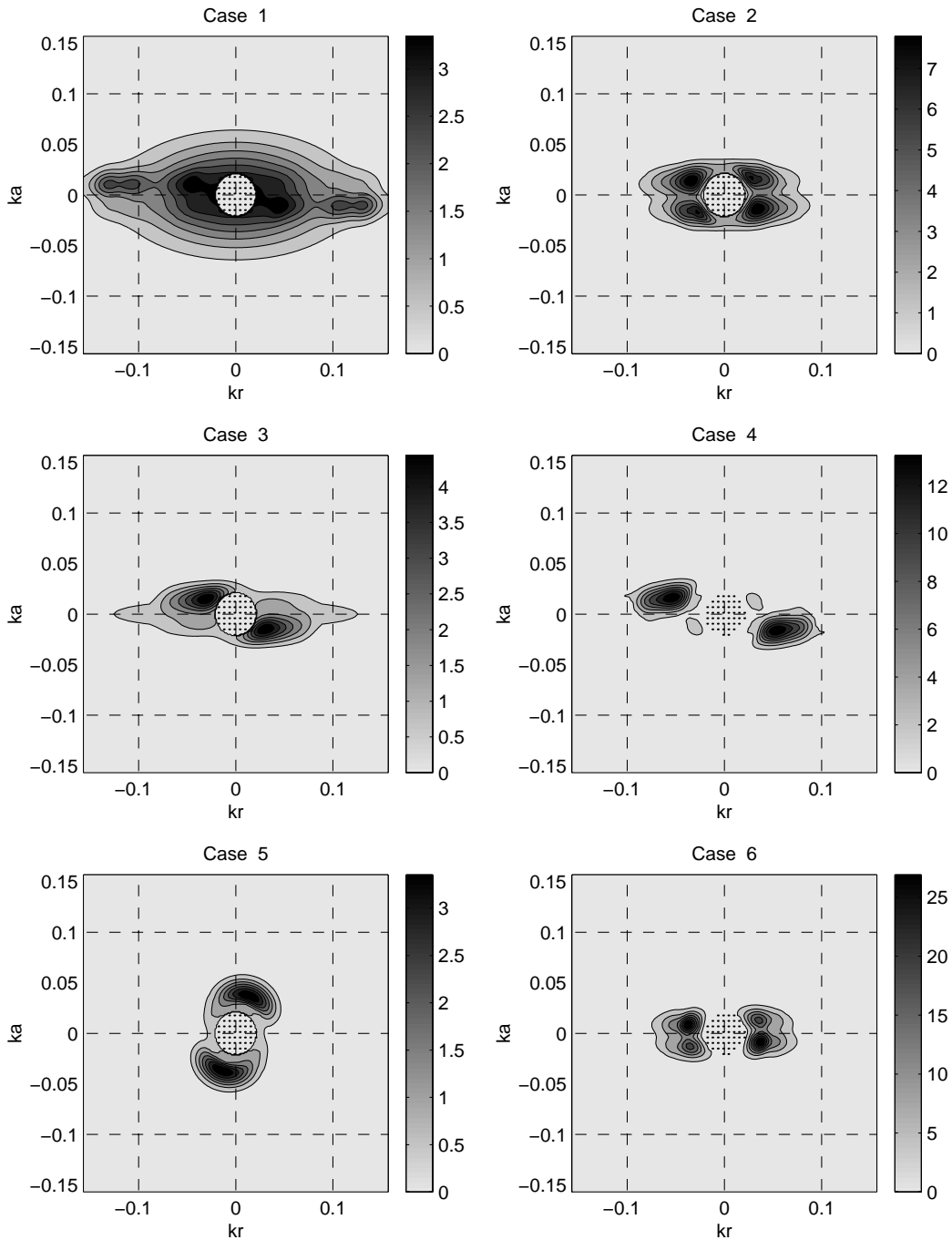
Figure 7: The real part of the modelled SAR cross-spectrum obtained based on the modified quasi-linear wave-SAR map and the buoy wave spectra. The axes follow Figure 1 and the grayscale represents the spectral density of the radar cross-section. Dotted areas follow Figure 2.
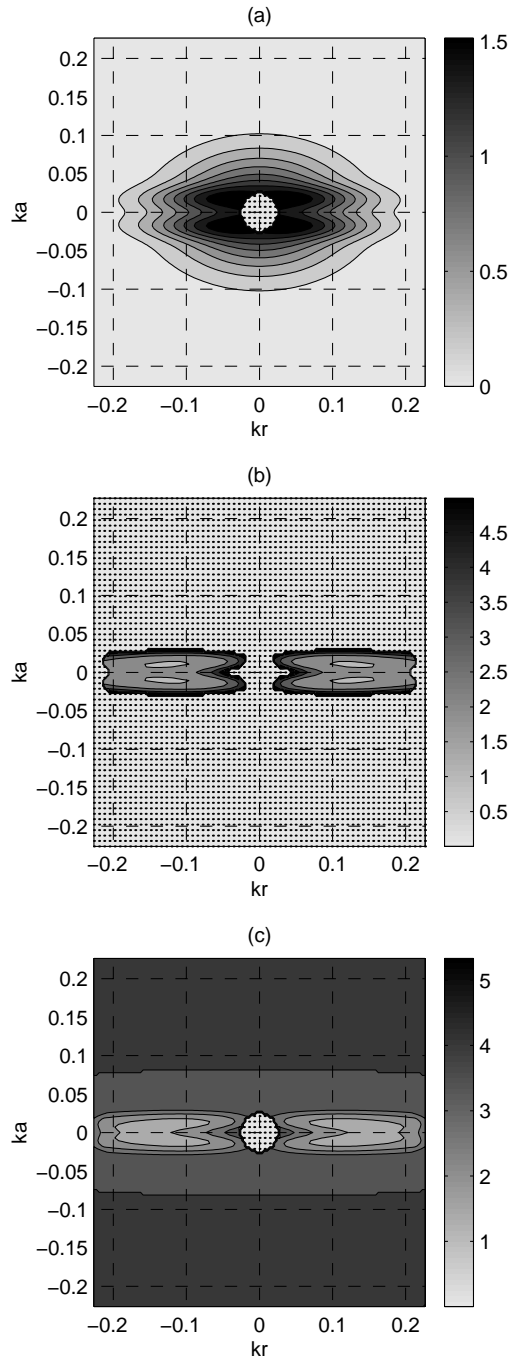
Figure 8: Typical RMS error variances (from case 1) for the following spectral quantities: (a) Residual between the simulated and observed RADARSAT coincident spectrum, (b) Wave estimate recovered using SAR information only, (c) Wave estimate using SAR and a prior wave spectrum with $\sigma_p^2 = 5^2$. The axes follow Figure 1. Dotted areas identify null spaces of the inversion.
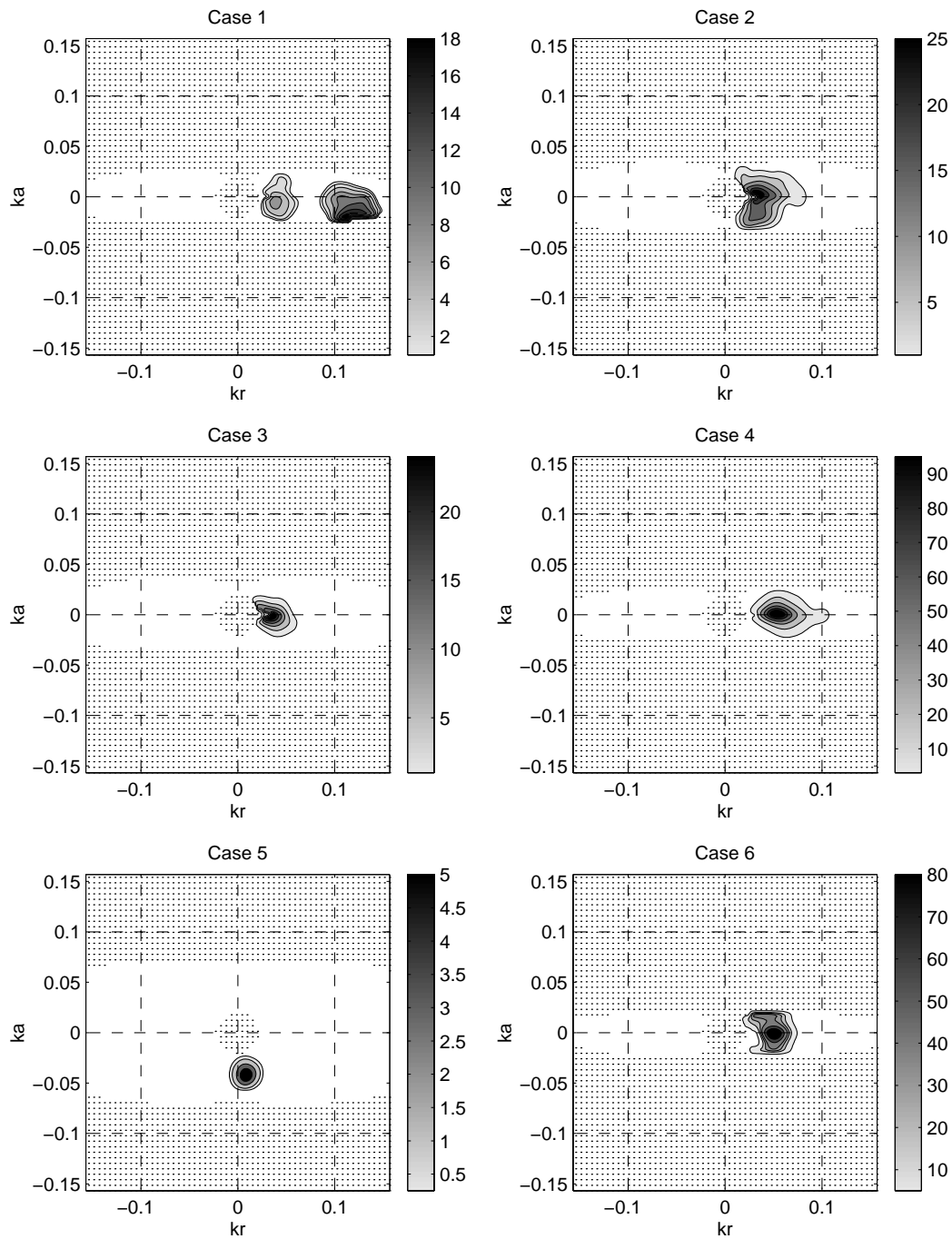
Figure 9: Wave estimates derived from RADARSAT SAR spectra. The axes follow Figure 1. The grayscale denotes the spectral density of the radar cross-section. Dotted areas identify null spaces of the inversion.
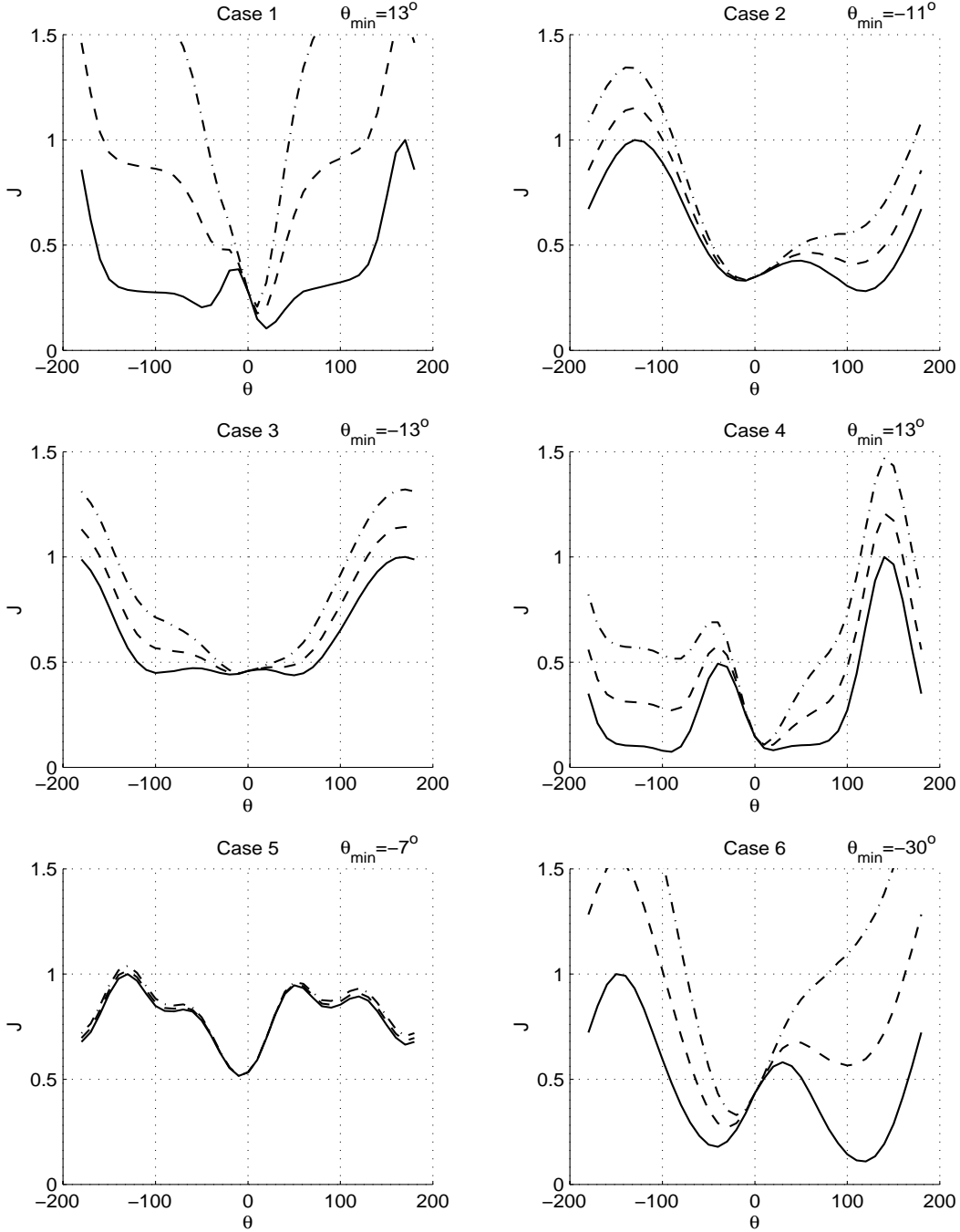
Figure 10: Cost function J as a function of the rotation angle θ (see text). The rotation angle is measured positive clockwise in degrees. Lines designate the three different treatments: baseline case with $\sigma_p^{-2} = 0$ (solid), weak regularization with $\sigma_p^{-2} = 15^{-2}$ (dashed), and strong regularization with $\sigma_p^{-2} = 10^{-2}$ (dash-dot). θ_{min} refers to the optimal rotation angle for the minimum J in the case of weak regularization.